Towards a new understanding of optical poling efficiency in multimode fibers

Maxime Jonard, Maggy Colas, Yann Leventoux, Tigran Mansuryan, Julie Cornette, et al.

Maxime Jonard, Maggy Colas, Yann Leventoux, Tigran Mansuryan, Julie Cornette, Alessandro Tonello, Stefan Wabnitz, Mario Zitelli, Fabio Mangini, Mario Ferraro, Yifan Sun, Sébastien Février, Jean-René Duclère, Vincent Couderc, Claire Lefort, "Towards a new understanding of optical poling efficiency in multimode fibers," Proc. SPIE 12143, Nonlinear Optics and its Applications 2022, 1214303 (25 May 2022); doi: 10.1117/12.2621278

SPIE.

Event: SPIE Photonics Europe, 2022, Strasbourg, France

Towards a new understanding of optical poling efficiency in multimode fibers

Maxime Jonard[a], Maggy Colas[b], Yann Leventoux[a], Tigran Mansuryan[a], Julie Cornette[b], Alessandro Tonello[a], Stefan Wabnitz[c,d], Mario Zitelli[c], Fabio Mangini[e], Mario Ferraro[c], Yifan Sun[c], Sébastien Février[a,] Jean-René Duclère[b], Vincent Couderc[a], Claire Lefort[a]

[a]XLIM Research Institute, UMR CNRS 7252, Université de Limoges, France; [b]IRCER, UMR CNRS 7315, Université de Limoges, France; [c]DIET, Sapienza University of Rome, Via Eudossiana 18, Rome, Italy; [d]CNR-INO, Istituto Nazionale di Ottica, Via Campi Flegrei 34, 80078 Pozzuoli (NA), Italy; [e]Dipartimento di Ingegneria dell'Informazione, Università di Brescia, via Branze 38, Brescia, Italy

ABSTRACT

All-optical poling was demonstrated for the first time in 1986 in single mode fibers: such nonlinear optical process enabled the introduction of a second-order susceptibility ($\chi^{(2)}$) in a doped silica fiber. By simply using an intense laser source, all-optical poling, later theoretically described by Stolen and coworkers, permitted the generation of a second harmonic (SH) signal in an otherwise centrosymmetric doped material. More recently, similar experiments have been carried out by exploiting complex beam propagation in multimode fibers. In this work we reveal, for the first time to our knowledge, the 3D spatial distribution of a $\chi^{(2)}$ nonlinearity written in a graded-index (GRIN) multimode (MM) fiber. In particular, the presence of a doubly-periodic distribution of $\chi^{(2)}$ is unveiled by means of multiphoton microscopy. The shortest period (tens of micrometers) is due to the beating between the fundamental and the SH beams, and it is responsible for their quasi-phase matching (QPM). Whereas the longest period (hundreds of micrometers) is associated with the periodic evolution, or self-imaging, of the power density of the MM beam along the GRIN MM fiber. The complex modal beating, leading to spatial self-cleaning of the fundamental beam, is thus printed inside the fiber core, and revealed by our measurements. We considered two fibers of similar composition and opto-geometric parameters, and we compared the evolution of the optical poling process with time. Despite the rather similar fiber characteristics, we observed a striking difference in the poling efficiency between the two fibers. Such observation led us to point out the importance of considering the complete fiber fabrication process (both the preform elaboration and the drawing steps) on the final structure and microstructure of optical fibers.

1. INTRODUCTION

Optical fibers are commonly composed by amorphous silica glass, and their centrosymmetric nature forbids the efficient generation of a SH by using a laser at fundamental frequency (FF). However, in 1986, Österberg described for the first time the nonlinear effect which is induced by the optical poling mechanism [1]. In the following year, he showed how the writing of a second-order susceptibility ($\chi^{(2)}$) in the fiber core can lead to a QPM mechanism [2]. After such a major breakthrough, Stolen, Djanov, and Balakirev, theoretically described the phenomenon of SH generation in optical fibers [3,4,5]. In particular, they showed how the susceptibility $\chi^{(2)}$ is not homogeneously distributed along the fiber, since it is associated with the coherent periodic beating between a fundamental and its second harmonic. More recently, several groups have demonstrated the impact on SH generation of the optical poling mechanism in Ge-doped MM fibers, and its connection with the spatial self-cleaning effect at the FF and SH wavelengths [6-9]. The study and understanding of nonlinear effects in MM fibers has recently regained considerable interest. Indeed, MM fibers are a cheap, easily accessible and ideal platform for the observation of new nonlinear phenomena, such as multimode solitons, Raman effect, geometric

Nonlinear Optics and its Applications 2022, edited by Neil G. R. Broderick, John M. Dudley, Anna C. Peacock, Proc. of SPIE Vol. 12143, 1214303 · © 2022 SPIE
0277-786X · doi: 10.1117/12.2621278

parametric instabilities (GPI), spatial Kerr self-cleaning, and optical wave condensation [10-16]. Quasi-single-mode second harmonic generation in MM fibers can be also added to the list of these novel processes.

Nonlinear MM fiber optics is at the basis of a series of wave mixing mechanisms, leading to the creation of new frequencies. We show here that SH generation can be controlled by managing the optical poling process in MM fibers. This scenario also raises new questions: how a periodically poled second-order nonlinearity can compete and coexist with third-order spatial and spectro-temporal processes, such as Kerr self-cleaning, GPI generation, and soliton dynamics? Thus, a complete understanding of the physical phenomena that occur during the optical poling is a key issue for controlling the process of new frequency generation via the mixing of $\chi^{(2)}$ and $\chi^{(3)}$ nonlinearities.

In this paper, we describe experiments based on the optical poling of two MM Ge-doped GRIN fibers. The two fibers, which are produced by two different manufacturers (Thorlabs and Alcatel), have the same core and cladding diameters (50/125 µm). The refractive index difference between the core and the cladding is also the same, and in both fibers it is realized by Ge dopants. Although the poling process followed the same protocol, the two fibers showed two radically different SH conversion efficiencies. More specifically, in the case of the 50/125 µm MM fiber provided by Thorlabs, no significant SH signal was observed at the fiber output. Whereas by using the Alcatel MM fiber, optical poling led to 1% SH conversion efficiency. Our research focuses on the origin of this difference between those two, nominally identical, germanium-doped fibers. We first performed a characterization of the second-order nonlinearity in the core of the optical fibers by means of longitudinal multiphoton microscopy, in particular for detecting the local SH generation. Thus, for the first time the $\chi^{(2)}$ inscription resulting from poling processing combined with spatial self-imaging (SSI) was experimentally visualized [17]. We completed this study by analyzing the core and cladding properties of the two fibers by means of energy dispersive X-ray spectroscopy (EDS) and Raman spectroscopy. We demonstrated that the poling efficiency is directly dependent on the silica structures, and more precisely on the different size of SiO_2 rings, which compose the glass after fiber drawing. We also measured the competition between the different frequency conversion processes such as GPI, SH, and third-harmonic generation (THG).

2. MATERIALS AND METHODS

Figure 1 illustrates the experimental setup used for our poling experiments. A Nd:YAG laser delivers 740 ps pulses with a central wavelength fixed at 1064 nm. The average power is 1.5 W, with a repetition rate of 27 kHz. Such a system delivers peak powers up to 75 kW for 56 µJ of energy per pulse. This input beam is coupled into the two-meter-long Ge-doped MM-GRIN fibers. Two Ge-doped MM-GRIN fibers with 50 µm core diameters and provided by two different manufacturers (Thorlabs and Alcatel), have been used for carrying out the comparative analysis. The laser beam is coupled into the MM-GRIN fibers by using a convergent lens of 8 mm of focal length, moved by a three-axis mechanical mount. The average power of the laser source and the input polarization beam state are controlled by two half-wave plates ($\lambda/2$) and a polarizer cube. A CCD camera with two bandpass filters (1064 nm, 10 nm FWHM and 532 nm, 10 nm FWHM) allows to record the spatial beam profile at FF and SH. A power meter, jointly with optical filters are used to record the average output power. A type-II KTP crystal, cut for second harmonic generation at 1064 nm, is placed before the optical fiber to initiate the poling process. After initial feeding, the KTP is removed, and the poling is left to grow larger by using only the initial SH which is created in the first centimeters of the MM fiber.

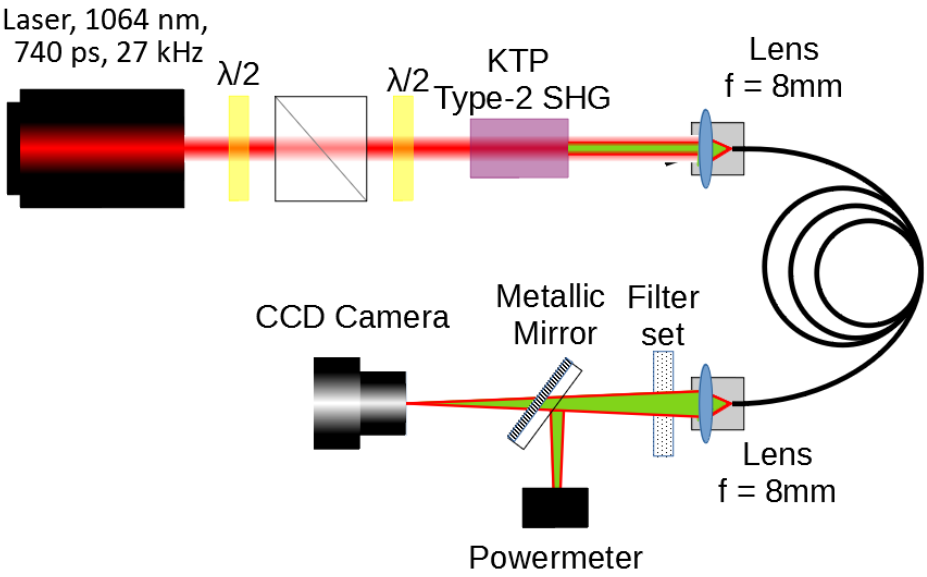

Figure 1. Experimental setup for all-optical poling of MM GRIN fibers.

2.1 Experimental characterization of optical poling along the fiber

The characterization of the writing effect associated with the poling process was carried out along the fiber by means of multiphoton microscopy. The inscription of a $\chi^{(2)}$ susceptibility in the core of the fiber can be detected by measuring the second harmonic light, which is side-emitted when launching femtosecond pulses in a direction which is perpendicular to the fiber axis. This characterization method is often used in microscopy, in order to image biological samples containing non-centrosymmetric structures, such as collagen or myosin. We used a commercial Olympus multiphoton microscope (BX61WI) coupled with a tunable titanium-doped sapphire (Ti:Sa) femtosecond laser system (Chameleon Ultra II, Coherent Inc). The excitation wavelength was set at 810 nm, and the detection was performed by a photomultiplier tube (PMT) combined with a detection filter centered at 405 nm, with a spectral width of 10 nm and a dichroic mirror (650 nm). We used two microscope objectives: the first was a Nikon objective with a large field of view (MRH00101, 10X, 0.3), whereas the second was an Olympus objective (XLPLN25XWMP, 25×, NA 1.05, W). A 2D translation stage allowed us to explore the sample with the infrared laser, in order to create 2D images at different optical planes. Sequential acquisitions of 2D image stacks combined with axial scanning (the microscope objective was moved by steps of 1 μm), permitted us to reconstruct the 3D distribution of the $\chi^{(2)}$ nonlinearity.

2.2 Characterization of the chemical composition of the core by electron microscopy

We use a chemical analysis electron microscope in order to obtain the features of the two fibers. Energy dispersive X-ray spectroscopy allows for determining the chemical composition of the samples. We carried out a profile analysis of the two fibers. In Figure 2, we may notice a parabolic evolution of the Germanium ions, leading to the parabolic refractive index profile of the MM fiber. Qualitatively the Germanium and Silicon content are the same between the two fibers, which is coherent with an identical nominal value of Δn of 0.015.

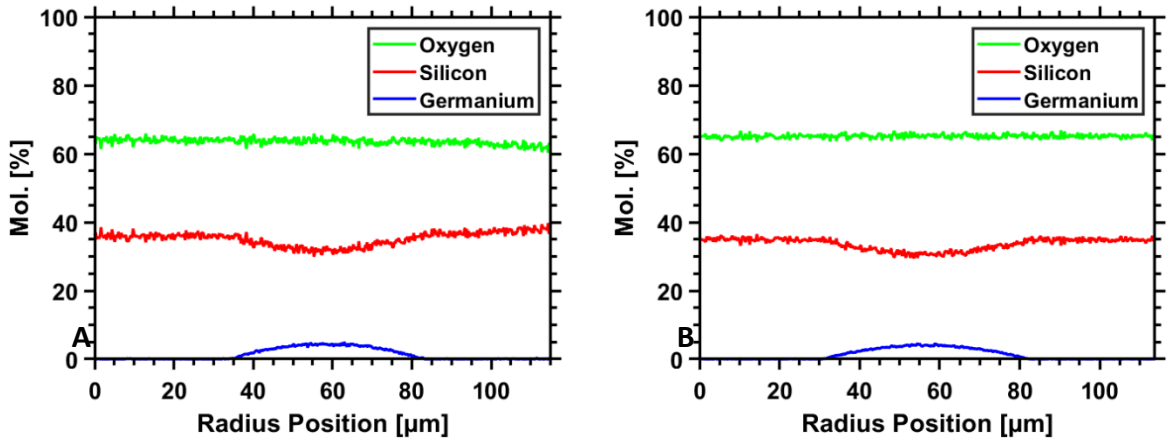

Figure 2. Molecular profile of chemical elements within the diameter of the two fibers. A. Chemical distribution of the 50/125 fiber from Thorlabs B. Chemical distribution of the 50/125 fiber from Alcatel.

3. EXPERIMENTAL RESULTS

3.1 Optical Poling of a 2-meters-long MM-GRIN fiber from Alcatel

In the case of the Alcatel fiber (drawn from a preform elaborated by the Modified Chemical Vapor Deposition (MCVD) process), optical poling successfully led to efficient SH generation: 10 mW of SH average power was obtained for 1 W of FF average power, reaching in these conditions a maximum SH conversion efficiency of 1%. Figure 3 shows the evolution over time of the average power of the SH, which is measured at the fiber output. A maximum of SH is obtained after minutes of laser exposure, before the saturation of the optical poling.

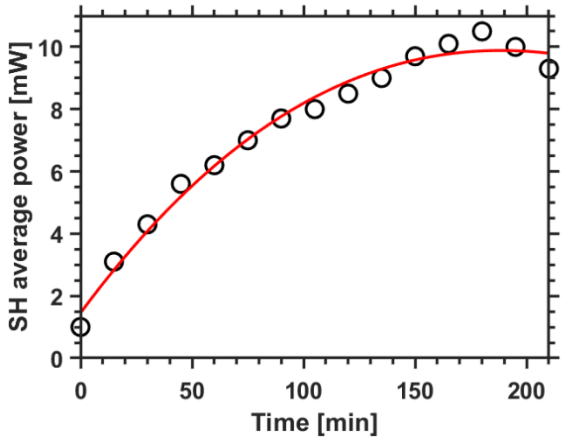

Figure 3. Optical poling of a 50/125 Alcatel MM-GRIN fiber. The red line is a guide for the eyes, to evidence the SH signal saturation.

3.2 Characterization of the poling structure by multiphoton imaging

The quadratic nonlinearity inscription into the fiber core was revealed, thanks to a standard multiphoton microscope. The measurement was realized in the first 40 cm of the optical fiber, where the spatial self-cleaning effect of the FF MM beam was not yet obtained. The complex $\chi^{(2)}$ structures, which result from the poling process in the presence of MM beam propagation, are clearly visible in Figure 4a. The spatial self-imaging showing the periodic replication of the transverse spatial distribution of a beam is experimentally illustrated here for the first time in our knowledge. We can still observe the presence of a short-scale beating period, which creates a local $\chi^{(2)}$ leading to SH generation peaks, approximately spaced

by 20 µm. Because of the parabolic refractive index profile of the fiber, beam self-imaging occurs in the MM fiber, which leads to a modulation of the amplitude of the second-order nonlinearity with a periodicity close to 0.55 mm. The same measurements have also been carried out at distances further down the fiber, where spatial self-cleaning takes place. Here the poling profile is significantly more uniform: a more regular distribution of $\chi^{(2)}$ results, owing to the dominant contribution of the fundamental mode (see Figure 4b). Consequently, the transverse near-field profiles of both the output fundamental and SH beam exhibit a bell shape (see insets in the figure 4).

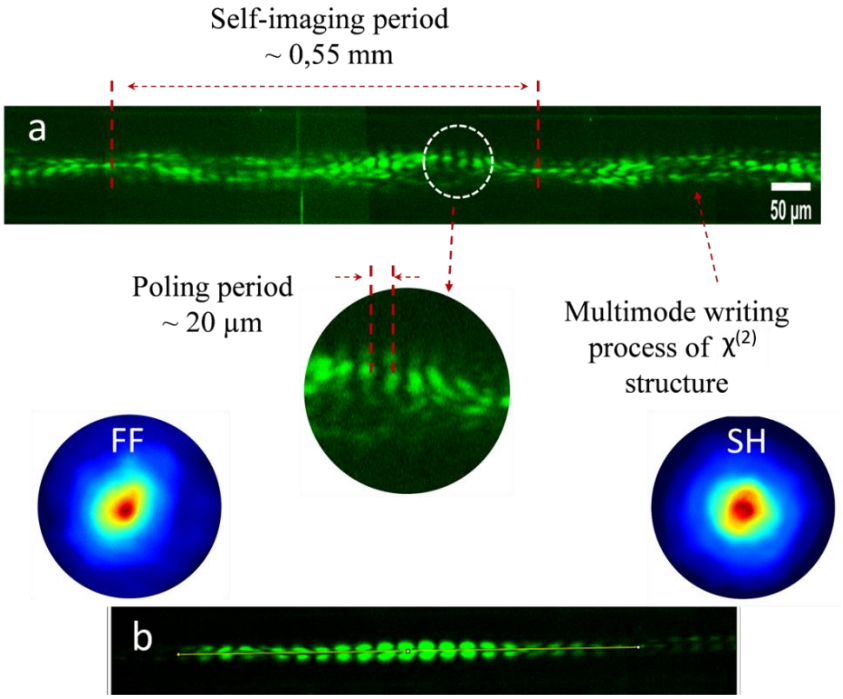

Figure 4. Experimental characterization of the $\chi^{(2)}$ nonlinearity written into the Alcatel optical fiber by using multiphoton microscope. a, image of the $\chi^{(2)}$ nonlinearity distribution in the first 40 cm of the fiber, i.e., before the Kerr self-cleaning process takes place; b image of the $\chi^{(2)}$ nonlinearity distribution in the fiber after the occurrence of spatial self-cleaning. Insets: images of the output beam near-fields for FF and SH beams.

The second-order nonlinear conversion is obtained thanks to a mechanism of QPM between FF and SH, which is introduced by the periodic inscription of the $\chi^{(2)}$. The transverse distribution of the second-order nonlinearity is also modulated by the self-imaging process [18]: the experimental period of $\xi_{experimental}$ = 550 µm is consistent with the theoretical period of $\xi_{theoretical}$ = 545 µm [17]. Thus, for the first time, the presence of poling could be directly visualized inside the MM fiber core, which highlights the role of charge displacements under the effect of the optical field beating. The results of Figure 4 experimentally confirm the complex distribution of $\chi^{(2)}$, and also provide an experimental proof of the spatial MM evolution of the FF beam towards a spatially clean profile.

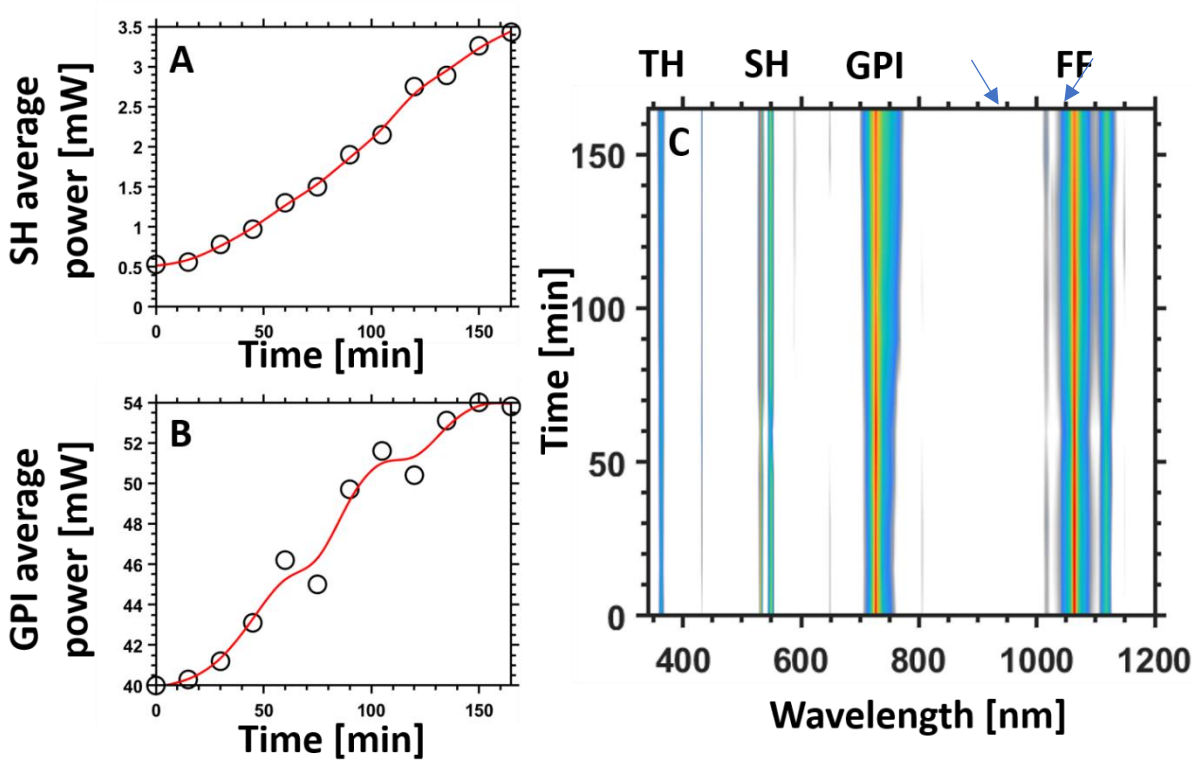

Figure. 5. Spectral analysis of all of the wavelength conversion phenomena observed during the poling process in the Alcatel MM GRIN optical fiber. A and B show the average power of SH (top) and GPI (bottom) versus the poling time. C illustrates the evolution of all of the wavelengths which are observed at the fiber output, vs. the poling time.

Besides SH generation, as shown in Figure 5, we also observed other processes that lead to conversion of the FF into other wavelengths. In figure 5C, the fundamental beam is framed by two lateral lines, representing the Stokes and the anti-Stokes lines of Raman conversion. Generation of GPI is also visible close to 735 nm, which represents the anti-Stokes line of the first-order conversion. Finally, the wavelength at 355 nm represents the third-harmonic generation of the FF pump beam. Because of these multiple frequency conversions, it is clear that the poling process competes with several other nonlinear effects, each of them depleting the initial pump, and limiting the writing of a second-order nonlinearity.

3.3 Optical Poling of a 2-meters-long MM-GRIN fiber from Thorlabs

We performed a second set of experiments under the same experimental conditions as in subsections 3.1 and 3.2. We used the 50/125 Ge-doped MM-GRIN fiber from Thorlabs (drawn from a preform elaborated by the Outside Vapor Deposition (OVD) process). The same poling protocol was implemented in all of the experiments. In this case, the average SH power measured at the output of the 2-meters long MM-GRIN fiber was very low when compared with the previous results obtained with the Alcatel fiber. The average SH power was at best 0.1 mW, indicating a failure of the poling process. As expected, the multiphoton microscope images did not reveal any significant second-order nonlinearity.

3.4 Analysis of the local structure of optical fibers by Raman spectroscopy

In order to elucidate the reason for such a significant difference in the poling process efficiency, we carried out a complementary investigation for each fiber. Specifically, we characterized the local structure (short and medium range orders) of the fiber core by means of Raman spectroscopy. Figure 6 illustrates the Raman spectra that were recorded for the two fibers. One can appreciate a clear difference in the spectrum at three distinct wave numbers: below 400 cm^{-1}, which is representative of the largest tetrahedron rings, at 489 cm^{-1}, which is representative of the 4 tetrahedron rings, and at 606

cm^{-1}, which is representative of the 3 tetrahedron rings [19]. Thus, despite the same Ge doping and opto-geometric parameters, these vibrational spectroscopy data testify to a slight difference in the local structure of these two fibers, which might be at the origin of the different poling efficiencies [20]. More specifically, it is reasonable to connect all that to the different overall processes undergone for the production of the two MM GRIN fibers, *i.e*. different methods employed for the fabrication of the preform (MCVD vs OVD) and different fiber drawing conditions [21,22].

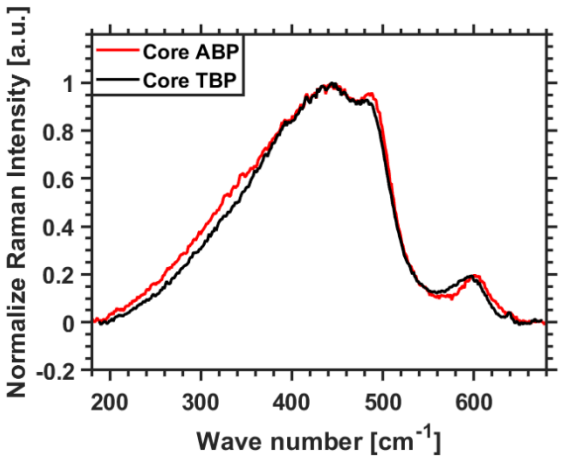

Figure 6. Raman spectra collected at the central part of the core for the two MM fibers. ABP and TBP respectively stands for Alcatel and Thorlabs Before Poling.

4. CONCLUSION

The optical poling technique has recently regained interest for the generation of new spectral frequencies by using MM fibers. In the present work, we have revealed that a drastic difference in the poling efficiency may exist between two nominally identical fibers. These MM fibers are provided by two different fiber suppliers (Thorlabs and Alcatel), but otherwise exhibit the same chemical composition and similar opto-geometric parameters. In particular, it was only possible to observe a clear generation of SH, during the time of exposure of the poling process, when using the Alcatel fiber. The imprinted second-order nonlinearity has been experimentally visualized by using a multiphoton microscope, which permits to reveal its complex distribution along the fiber, as a result of MM propagation along the initial fiber section. When repeating the same characterization at the fiber end, we obtained a much more uniform distribution. Here, the poling process was mainly driven by the presence of a Kerr self-cleaning process for both the FF and the SH. Such regularity in the local writing process may, in turn, provide a clear proof of the presence of the spatial self-cleaning process which is obtained along GRIN optical fibers. The experimental analysis carried out through EDS and spontaneous Raman scattering spectra measurements has guided our reasoning towards the impact of the internal structure and microstructure of the material, for explaining the observed drastic difference in poling efficiency between the two MM fibers. All this will be commented in details in a forthcoming full article.

ACKNOWLEDGEMENTS

We acknowledge the financial support of the following grants: Agence Nationale de la Recherche (ANR-10-LABX-0074-01, ANR-18-CE080016-01); Horizon 2020 EU programme via the European Research Council Advanced Research Grant (740355); Ministero dell'Istruzione, dell'Universit`a e della Ricerca
(R18SPB8227); As well, this work was supported by institutional grants from the LabEX SigmaLim (ANR-10-LABX-0074-01) and benefited of some fundings via both the TRAFIC project (ANR-18-CE08-0016-01) and the F2MH project (AAP NA 2019-1R1M01).

REFERENCES

[1] U. Osterberg and W. Margulis, “Dye laser pumped by Nd:YAG laser pulses frequency doubled in a glass optical fiber”, Optics Letters, 11 (8), 516-518 (1986)

[2] U. Osterberg and W. Margulis, “Experimental studies on efficient frequency doubling in glass optical fibers”, Optics Letters, 12 (1), 57-59 (1986)

[3] R. H. Stolen and H. W. K. Tom, “Self-organized phase-matched harmonic generation in optical fibers”, Optics Letters, 12 (8), 585-587 (1987)

[4] E. M. Dianov, D. S. Starodubov, “Photoinduced generation of the second harmonic in centrosymmetric media”, Quantum Electronics, 25 (5), 395-407 (1995)

[5] M.K. Balakirev, L.I. Vostrikova, V.A. Smirnov, “Efficiency of optical poling of isotropic media”, Quantum Electronics, 38 (8), 724-730 (2008)

[6] A. B. Grudinin, E. Dianov, D. Korbkin, A. M. Prokhorov, and D. Khaidarov, “Nonlinear mode coupling in multimode optical fibers; excitation of femtosecond range stimulated-Raman-scattering solitons”, JETP Letters, 47, 356-359 (1988).

[7] M. A. Eftekhar, Z. Sanjabi-Eznaveh, J. E. Antonio-Lopez, F. W. Wise, D. N. Christodoulides, and R. Amezcua-Correa, “Instant and efficient second-harmonic generation and down-conversion in unprepared graded-index multimode fibers”, Optics Letters, 42 (17), 3478-3481 (2017).

[8] D. Ceoldo, K. Krupa, A. Tonello, V. Couderc, D. Modotto, U. Minoni, G. Millot, and S. Wabnitz, “Second harmonic generation in multimode graded-index fibers: spatial beam cleaning and multiple harmonic sideband generation”, Optics Letters, 42 (5), 971-974 (2017).

[9] K. Krupa, A. Tonello, A. Barthélémy, T. Mansuryan, V. Couderc, G. Millot, P. Grelu, D. Modotto, S. A. Babin, and S. Wabnitz, “Multimode nonlinear fiber optics, a spatiotemporal avenue”, APL Photonics 4, 110901 (2019).

[10] Z. Zhu, L. G. Wright, D. N. Christodoulides, and F. W. Wise, “Observation of multimode solitons in few-mode fiber,” Opt. Lett. 41, 4819-4822 (2016).

[11] K. Krupa, A. Tonello, A. Barthélémy, V. Couderc, B. M. Shalaby, A. Bendahmane, G. Millot, and S. Wabnitz, “Observation of geometric parametric instability induced by the periodic spatial self-imaging of multimode waves,” Phys. Rev. Lett. 116, 183901 (2016).

[12] K. Krupa, A. Tonello, B. M. Shalaby, M. Fabert, A. Barthélémy, G. Millot, S. Wabnitz, and V. Couderc, “Spatial beam self-cleaning in multimode fibres,” Nat. Photonics 11(4), 237–241 (2017).

[13] E. V. Podivilov, D. S. Kharenko, V. A. Gonta, K. Krupa, O. S. Sidelnikov, S. Turitsyn, M. P. Fedoruk, S. A. Babin, and S. Wabnitz, “Hydrodynamic 2D turbulence and spatial beam condensation in multimode optical fibers,” Phys. Rev. Lett. 122, 103902 (2019).

[14] A. Fusaro, J. Garnier, K. Krupa, G. Millot, and A. Picozzi, “Dramatic acceleration of wave condensation mediated by disorder in multimode fibers," Phys. Rev. Lett. 122, 123902 (2019).

[15] Z. Liu, L. G. Wright, D. N. Christodoulides, and F. W. Wise, “Kerr self-cleaning of femtosecond-pulsed beams in graded-index multimode fiber,” Opt. Lett. 41(16), 3675–3678 (2016).

[16] L. G. Wright, Z. Liu, D. A. Nolan, M.-J. Li, D. N. Christodoulides, and F. W. Wise, “Self-organized instability in graded-index multimode fibres,” Nat. Photonics 10(12), 771–776 (2016).

[17] T. Hansson, A. Tonello, T. Mansuryan, F. Mangini, M. Zitelli, M. Ferraro, A. Niang, R. Crescenzi, S. Wabnitz, and V. Couderc, “Nonlinear beam self-imaging and self-focusing dynamics in a GRIN multimode optical fiber: theory and experiments”, Optics Express, 28(16), 24005 (2020).

[18] F. Mangini, M. Ferraro, M. Zitelli, A. Niang, A. Tonello, V. Couderc, O. Sidelnikov, F. Frezza, and S. Wabnitz “Experimental observation of self-imaging in SMF-28 optical fibers”, Optics Express, 29(8), 12625 (2021).

[19] C. Martinet, V. Martinez, C. Coussa, B. Champagnon, M. Tomozawa, “Radial distribution of the fictive temperature in pure silica optical fibers by micro-Raman spectroscopy”, Journal of Applied Physics, 103 (8), 083506 (2008)

[20] M. Lancry, E. Régnier, and B. Poumellec, “Fictive temperature in silica-based glasses and its application to optical fiber manufacturing”, Progress in Materials Science, 57(1), 63-94. (2012)

[21] A. E. Geissberger, F. L. Galeener, “Raman studies of vitreous SiO2versus fictive temperature”, Physical Review B, 28 (6), 3266-3271 (1983)

[22] M. J. Tomozawa, “Optical Fiber Reliability and Testing”, Proceedings of SPIE, 3848 (1999)